Plasmonic nano-comb structures for efficient large-area second harmonic generation

Hongchul Sim,[1] Hee-Jin Lim,[1] Jung-Hwan Song,[1] Myung-Ki Kim,[1,*] and Yong-Hee Lee[1,2]

[1]*Department of Physics, KAIST, Daejeon 305-701, South Korea*
[2]*yhlee@kaist.ac.kr*
[*]*kmk1852@kaist.ac.kr*

Abstract: We propose and demonstrate plasmonic nano-comb (PNC) structures for efficient large-area second-harmonic generation (SHG). The PNCs are made of 250 nm-thick gold film and have equally-spaced 30 nm-slits filled with ploy vinylidene fluoride-co-trifluoroethylene (P(VDF-TrFE)). The PNC with 1.0 μm-spacing couples resonantly with 1.56 μm 100-fs laser beams. For the 1.0 μm-spacing PNCs under the fixed-pump-power condition, the nonlinear SHG power remains almost independent of the pump diameter ranging from 2 μm to 6 μm. The SHG power from the resonant PNC is measured to be 8 times larger than that of the single-nano-gap metallic structure, when the pump beam is tightly-focused to 2 μm in diameter in both cases. This relative enhancement of the total nonlinear SHG signal power reaches up to >200 when the pump beam diameter is increased to 6 μm. We attribute this unusual phenomenon to the resonant coupling of the finite-size pump wave with the finite-size one-dimensional plasmonic mode.

OCIS codes: (190.0190) Nonlinear optics; (240.6680) Surface plasmons.

References and links

1. L. Novotny and N. van Hulst, "Antennas for light," Nat. Photon. **5**(2), 83–90 (2011).
2. J. A. Schuller, E. S. Barnard, W. Cai, Y. C. Jun, J. S. White, and M. L. Brongersma, "Plasmonics for extreme light concentration and manipulation," Nat. Mater. **9**(3), 193–204 (2010).
3. A. Kinkhabwala, Z. Yu, S. Fan, Y. Avlasevich, K. Müllen, and W. E. Moerner, "Large single-molecule fluorescence enhancements produced by a bowtie nanoantenna," Nat. Photon. **3**(11), 654–657 (2009).
4. W.-H. Chao, R.-J. Wu, C.-S. Tsai, and T.-B. Wu, "Surface plasmon-enhanced emission from metal-island-coated YAG:Ce thin-film phosphor," J. Electrochem. Soc. **156**(12), J370–J374 (2009).
5. A. Nahata, R. A. Linke, T. Ishi, and K. Ohashi, "Enhanced nonlinear optical conversion from a periodically nanostructured metal film," Opt. Lett. **28**(6), 423–425 (2003).
6. W. Cai, J. S. White, and M. L. Brongersma, "Compact, high-speed and power-efficient electrooptic plasmonic modulators," Nano Lett. **9**(12), 4403–4411 (2009).
7. S. Kim, J. Jin, Y.-J. Kim, I.-Y. Park, Y. Kim, and S.-W. Kim, "High-harmonic generation by resonant plasmon field enhancement," Nature **453**(7196), 757–760 (2008).
8. W. Cai, A. P. Vasudev, and M. L. Brongersma, "Electrically controlled nonlinear generation of light with plasmonics," Science **333**(6050), 1720–1723 (2011).
9. J. B. Jackson and N. J. Halas, "Surface-enhanced Raman scattering on tunable plasmonic nanoparticle substrates," Proc. Natl. Acad. Sci. U.S.A. **101**(52), 17930–17935 (2004).
10. K. Okamoto, I. Niki, A. Scherer, Y. Narukawa, T. Mukai, and Y. Kawakami, "Surface plasmon enhanced spontaneous emission rate of InGaN/GaN quantum wells probed by time-resolved photoluminescence spectroscopy," Appl. Phys. Lett. **87**(7), 071102 (2005).
11. R. A. Farrer, F. L. Butterfield, V. W. Chen, and J. T. Fourkas, "Highly efficient multiphoton-absorption-induced luminescence from gold nanoparticles," Nano Lett. **5**, 1139–1142 (2005).
12. N. Pfullmann, C. Waltermann, M. Noack, S. Rausch, T. Nagy, C. Reinhardt, M. Kovačev, V. Knittel, R. Bratschitsch, D. Akemeier, A. Hütten, A. Leitenstorfer, and U. Morgner, "Bow-tie nano-antenna assisted generation of extreme ultraviolet radiation," New J. Phys. **15**(9), 093027 (2013).
13. B. Ploss and B. Ploss, "Dielectric nonlinearity of PVDF–TrFE copolymer," Polymer (Guildf.) **41**(16), 6087–6093 (2000).
14. Lumerical Solutions, Inc., http://www.lumerical.com/tcad-products/fdtd/.

#209112 - $15.00 USD Received 28 Mar 2014; revised 24 Jun 2014; accepted 25 Jun 2014; published 7 Jul 2014

15. C. Forestiere, A. Capretti, and G. Miano, "Surface integral method for second harmonic generation in metal nanoparticles including both local-surface and nonlocal-bulk sources," J. Opt. Soc. Am. B **30**(9), 2355–2364 (2013).
16. R. W. Boyd, *Nonlinear Optics Second Edition* (Academic, 2003), Chap. 2.
17. S. A. Maier, *Plasmonics: Fundamentals and Applications* (Springer, 2007), Chap. 9.
18. G. F. Walsh and L. Dal Negro, "Enhanced second harmonic generation by photonic-plasmonic fano-type coupling in nanoplasmonic arrays," Nano Lett. **13**(7), 3111–3117 (2013).

1. Introduction

Various metallic nanostructures such as dipole/bowtie optical antennas [1–3], metal island films [4], and metallic nano-slits [5,6] have been studied because they enable us to funnel electromagnetic energy into a small space of deep-sub-wavelength scale. The resonantly-amplified electric field in the metallic nanostructure often enables the extraordinary enhancement of nonlinear optical effects [7,8] such as surface-enhanced Raman scattering [9], Purcell effect [10], and multi-photon photo-luminescence [11]. However, in practice, tight focusing onto an isolated metallic nano-structure results in unavoidable heat generation and temperature rise. Accordingly those metallic nanostructures made for nonlinear optical phenomena cannot escape from the issue of optical damage [12]. It is worthwhile looking into metallic nanostructures that could produce nonlinear optical signals efficiently over a broad area for a given incident pump power such that the thermal damage issue can be relieved.

Here, we propose and demonstrate the plasmonic nano-comb (PNC) structure as efficient, large-area nonlinear optical generator. When the PNC structure is resonantly coupled with finite-size incident pump beams, the nonlinear second-harmonic generation signal shows pump-size-independency over a range of pump diameters of 2~6 μm.

2. Plasmonic nano-comb structure

The PNC structure is composed of periodic metallic nano-slits as shown in Figs. 1(a) and 1(b). A 250 nm-thick gold layer is deposited on glass substrate by electron-beam evaporation and the PNC pattern is inscribed by focused ion-beam milling. The metallic slit profile that resembles a trapezoid is fabricated as shown in Fig. 1(c) where top and bottom gap widths are measured to be 100 nm and <30 nm, respectively. The area of the PNC used for the experiment is about 20 × 20 μm^2 which is much larger than the wavelength of interest, 1.56 μm. The gold nano-comb structures with different periodicities (p) are fabricated. In addition, the nano-metallic structure having just one nano-slit of identical milling profile is also prepared for comparison purposes. A polyvinylidene fluoride-co-trifluoroethylene (P(VDF-TrFE)) [13] is then coated over the patterned gold layer as an optical nonlinear medium.

The trapezoidal gap geometry turns out to be more advantageous in enhancing the electric field in the gap in comparison to the rectangular counterpart. For finite-difference time-domain (FDTD) computations [14], a trapezoidal mesa geometry approximating the fabricated sample is used with refractive indices of glass, P(VDF-TrFE), and gold as 1.5, 1.42 and 0.525 + 9.98i, respectively as shown in Fig. 1(d). The rectangular gap geometry is also analyzed for comparison, where the average value (65 nm) of the top width and the bottom width of the trapezoid is taken as the gap width. Figures 1(d) and 1(e) compare the field distributions in the trapezoidal and the rectangular gap slit structures. One can observe that the field in the trapezoidal slit is tightly localized near the bottom of the trapezoid where the gap width is smallest, while the field in the rectangular one is distributed over the gap area. The mode cross-sectional area along x-z plane for a trapezoidal gap is calculated to be 1.0×10^{-3} μm^2, while that of the rectangular gap is 7.0×10^{-3} μm^2. The respective maximum enhancements of E-field intensity are 510 and 150, for the trapezoidal and rectangular gap.

The sample is pumped from the air side of the Au film and the generated nonlinear optical signals are collected through the glass substrate as shown in Fig. 2(a). An 80-MHz 100

#209112 - $15.00 USD Received 28 Mar 2014; revised 24 Jun 2014; accepted 25 Jun 2014; published 7 Jul 2014

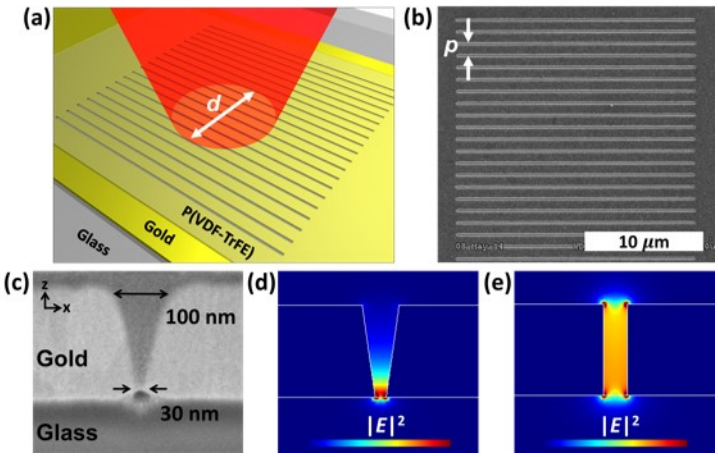

Fig. 1. (a) Schematic of a plasmonic nano-comb (PNC) structure. *d* is the pump beam diameter. SEM pictures of (b) top and (c) side views. *p* is the periodicity. $|E|^2$ profiles for (d) trapezoidal mesa geometry and (e) rectangular gap geometry by finite-difference time-domain computations.

-fs-pulse laser (Toptica FemtoFiber pro NIR) running at 1.56 μm is used as a pump source. Throughout our experiment the time-averaged incident pump power (P_ω) is fixed at 20 mW and only the pump spot size is varied. The peak power of the 100-fs pulse corresponds to 2.5 kW. A long-pass filter ($\lambda_{\text{cut-off}}$ = 1.2 μm) in front of the laser is inserted to remove the unwanted short-wavelength radiation from the pump laser. The pump beam is focused using a × 60 objective lens (NA = 0.65) and the spot size is controlled by looking at the incidence laser beam at the back focal plane of the objective lens. In this setup, variation of the spot size is limited from 2 μm to 6 μm to maintain the pump power constant.

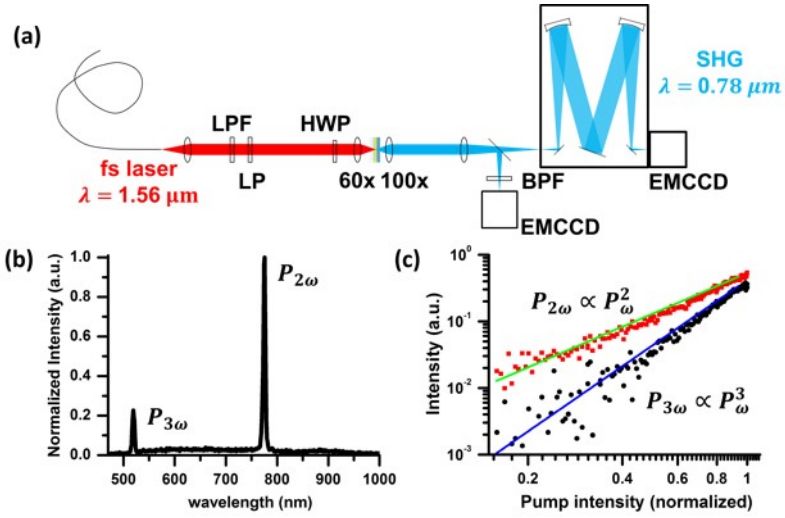

Fig. 2. (a) Schematic of measurement setup. (LPF: long pass filter, LP: linear polarizer, HWP: half wave plate, BPF: band pass filter), (b) Typical nonlinear signal spectrum, (c) Measured nonlinear signals as a function of pump intensity at 780 nm and 520 nm.

The polarization of the laser is set perpendicular to the slit orientation (*x*-polarization) to excite the slit antenna mode and the pumping spot is placed near the center of the pattern. The nonlinear optical signals are collected through the glass substrate by a × 100 oil immersion lens (NA = 1.40) which is expected to collect the major fraction of the nonlinear signal. To block the 1.56 μm pump laser transmitted through the metallic nano-comb structure, a short-

#209112 - $15.00 USD Received 28 Mar 2014; revised 24 Jun 2014; accepted 25 Jun 2014; published 7 Jul 2014

pass filter is put after the sample. The nonlinear optical signals are imaged by an electron-multiplication charge-coupled device (EMCCD) with a narrow band-pass filter (780 ± 5 nm for SHG) and also monitored by a spectrometer.

3. Experiment

A typical nonlinear optical spectrum generated from a PNC with 1.0 μm period is shown in Fig. 2(b). Two spectral peaks associated with the second harmonic generation (SHG; $P_{2\omega}$) and the third harmonic generation (THG; $P_{3\omega}$) are observed at 780 nm and 520 nm, respectively. The red and black dots in Fig. 2(c) are taken at 780 nm and 520 nm from the measured spectral data and the green and blue lines are from the fittings based on $y \propto x^2$ and $y \propto x^3$, respectively. Note that both pump power dependence and the wavelength of the nonlinear signal agree well with the expectation based on multi-photon processes.

Various plasmonic nano-comb structures of different spacing (spanning p = 500~1300 nm) are fabricated for the structural scanning. The resonant enhancement of SHG is observed from the 1.0-μm spacing PNC structure when pumped at a fixed wavelength of 1.56 μm in both measurement and FDTD simulation, as shown in Fig. 3(a). Bright second harmonic images are observed from the P(VDF-TrFE) regions in-between the nano-metal strips, as one can see in Fig. 3(c). In comparison, in the absence of P(VDF-TrFE) medium plasmonic nano-comb structures generate much weaker SHG signals. The measured second harmonic signal stems mainly from the nonlinear P(VDF-TrFE) and only partly from the metal itself [15].

For comparison purposes, the incident pump laser power is held constant and only the diameter of the pump laser beam is varied. The reference sample having only one nano-slit generates strong nonlinear signals when the pump spot is small. And as expected, it decreases monotonically with the pump spot diameter (d). However, it is interesting to observe that the maximum $P_{2\omega}$ obtainable from the single nano-slit is much weaker than $P_{2\omega}$ from the nano-comb structures. We would like to emphasize that the $P_{2\omega}$ obtained from the 1.0 μm-spacing PNC is over 8 times stronger than that of the single nano-slit even when focused to a 2.0 μm diameter.

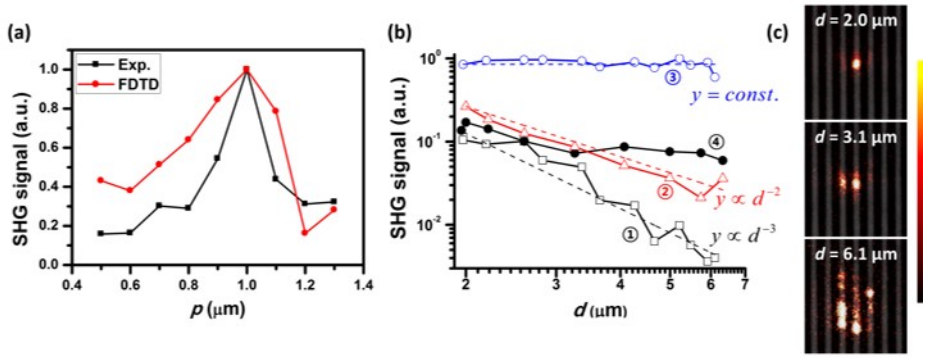

Fig. 3. (a) Structural scanning: $P_{2\omega}$ measured (black square line) and calculated (red circle line) as a function of spacing p with fixed d = 3.0 μm. (b) Measured $P_{2\omega}$ as a function of pump beam diameter d for ① a single slit and slit arrays with ② p = 0.5 μm, ③ 1.0 μm and ④ 1.5 μm (different samples from (a)). (c) Images of the second harmonics for pumping diameters of 2.0 μm, 3.1 μm and 6.1 μm, respectively.

As one can see in Fig. 3(b), the $P_{2\omega}$ from different nano-combs generally decreases with the pump spot size. However, it is interesting to see that the SHG signals from the 1.0 μm-spacing PNC remain almost independent of all the pump beam diameters ranging from 2 μm to 6 μm, once the pump power is fixed. Note in Fig. 3(b) that the SHG from this sample is > 200 times stronger than that from the reference single nano-slit sample when both samples are pumped with beams with identically large diameter of 6 μm. The second harmonic intensity profiles from the 1.0 μm-spacing PNC are plotted in Fig. 3(c), for three different beam diameters of 2.0, 3.1 and 6.1 μm. The scattered hot spots in this figure are attributed to the fluctuation of the metallic nano-gap, originating from the imperfect fabrication. From the

#209112 - $15.00 USD Received 28 Mar 2014; revised 24 Jun 2014; accepted 25 Jun 2014; published 7 Jul 2014

measured data, one can see that the $P_{2\omega}$ from the 0.5 μm-spacing PNC (red curve) varies with $1/d^2$ and that from the 1.5 μm-spacing PNC (black circled-curve) decreases more slowly than that of the 0.5 μm-spacing PNC.

4. Analyses and discussions

In general, for a uniform nonlinear medium pumped with a fixed incident power (P_ω), the $P_{2\omega}$ decreases linearly with pump area (Δa), because the irradiance of pump beam decreases with pump area. The $P_{2\omega}$ is described by the following relation [16,17].

$$P_{2\omega} = C_0 \left(P_\omega / \Delta a \right)^2 \Delta a_{nl} = D_0 \left(| E_{inc} |^2 \right)^2 \Delta a_{nl} \quad (1)$$

Here Δa_{nl} represents the effective area participating in the nonlinear process and C_0 and D_0 are proper respective constants. E_{inc} is the incident electric field in the nonlinear medium. For a uniform nonlinear medium the second harmonic signal usually becomes weaker with pump beam size as $1/\Delta a$ ($\sim 1/d^2$). However, for patterned nonlinear media, the situation is somewhat complicated and the E_{inc} should be replaced with the electric field in the nano-gap E_{gap}. For the one-dimensional single nano-slit filled with a nonlinear medium, the effective area (Δa_{nl}) increases linearly with pump beam diameter (d) while the irradiance decreases with Δa. So the resultant $P_{2\omega}$ shows $1/d^3$ dependence, as shown in Fig. 3(b).

In contrast, the experimental $P_{2\omega}$ of 1.0 μm-spacing PNCs can't be explained from this simple approach. In this case, the measured $P_{2\omega}$ remains nearly unchanged with respect to the pump beam size ranging from 2 μm to 6 μm. In the experiment, the pump beam covers more than one slit and Δa_{nl} increases nearly with d^2. In order to satisfy the constancy of $P_{2\omega}$, the $D_0(|E_{gap}|^2)^2$ term in Eq. (1) need to be a function of $1/d^2$ instead of $1/d^4$.

Mathematically speaking, the electric field intensity ($|E_{gap}|^2$) needs to decrease with the pump size d, if one wants to explain the constancy of $P_{2\omega}$. We attribute this unusual claim to the resonant coupling of the finite-size pump wave with the finite-size PNC structure. When the lattice constant (spacing) of one-dimensional PNC structure is close to the wavelength in the glass, the normally-incident wave is known to couple resonantly to the in-plane plasmonic mode [18]. It is confirmed through 3-D FDTD computations employing the Drude model of gold that the 1.0 μm-spacing PNC shows plasmonic resonance near 1.56 μm (Fig. 4(a)) and the $|E_{gap}|^2$ is strongly amplified in the metallic nano-gap, as shown in Figs. 4(a) and 4(b). Here the maximum enhancement of the electric field intensity in the nano-gap is found to be more than 500 times stronger than that of the incident pump beam. Physically speaking, the 1.0 μm-spacing PNC satisfying the resonance condition is able to store more electromagnetic energy than the other non-resonant counterparts.

In addition to the resonance effect, the modal overlap between the finite-size pump wave and the finite-size plasmonic mode is needed to explain the increase of $|E_{gap}|^2 / |E_{inc}|^2$ with beam size. The situation is easier to understand in the k-space (Fourier-transformed space). The plasmonic mode profile of the finite-size PNC in k-space is shown in Fig. 4(c) (yellow region). When the incident Gaussian pump beam diameter is smallest (2 μm), the width of pump wave in k-space (Δk_{pump}) is much broader than Δk_{PNC} (yellow region) and the overlap between two modes is not very good. In this case, although the $|E_{gap}|^2$ itself has the maximum value because of the tightest focusing, the total $P_{2\omega}$ is not any stronger than that obtainable from the broader pumping counterparts, because of the corresponding small active volume and the modal overlap. The modal overlap is found to increase with pump size as shown in Fig. 4(c).

We also find that the relative enhancement of electric field intensity $|E_{gap}|^2 / |E_{inc}|^2$ increases in a linear fashion with the pump diameter up to 10 μm and then saturates as shown in Fig. 4(b), which agrees with the tendency of the modal overlap integral in k-space. When the pump diameter is larger than 10 μm, Δk_{pump} becomes much smaller than Δk_{PNC} (yellow region) and the modal overlap becomes saturated. The incident electromagnetic energy is efficiently funneled into the plasmonic mode until the mode coupling is saturated. For the case of $d > 10$ μm, Fig. 4(b) shows the saturation of coupling between the incident pump beam and the PNC

#209112 - $15.00 USD Received 28 Mar 2014; revised 24 Jun 2014; accepted 25 Jun 2014; published 7 Jul 2014

mode. Therefore, $P_{2\omega}$ decreases with $1/d^2$, which is cross-examined through FDTD calculations as a function of d, as shown in Fig. 4(d).

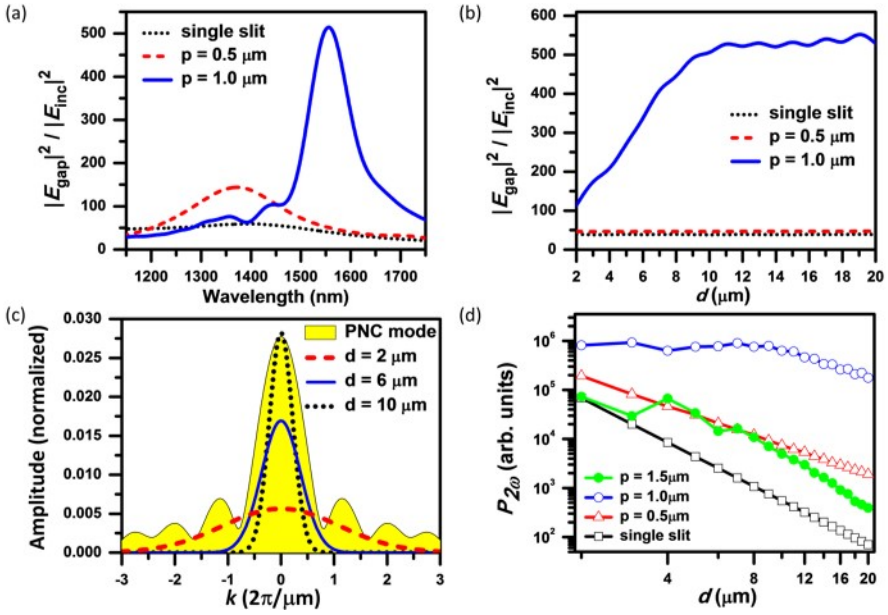

Fig. 4. (a) Relative enhancement spectra of electric field intensity in the nano-gap when d = 10 μm. (b) Relative enhancement of E-field intensity as a function of pump size. (c) k-space profiles of the plasmonic mode of 1.0-μm-spacing PNC and incident waves of different sizes. (d) Calculated total SHG powers as a function of d.

In comparison, the relative enhancement of electric field intensity in the nano-gap of the 0.5 μm-spacing PNC shows no resonance effect and remains weak and almost constant, independent of the pump size, as shown in Fig. 4(b). Thus the second harmonic signal of the 0.5 μm-spacing PNC shows $1/d^2$ dependence, as shown in Figs. 3(b) and 4(d). In this case, both the number and the length of nano-slits within the pump spot increases linearly with pump diameter. For the 1.5 μm-spacing PNC, the SHG power decreases monotonically with d in a more complicated fashion, as shown in Figs. 3(b) and 4(d). The 1.5 μm-spacing PNC shows no lateral coupling with nearest neighbors and no resonant behaviors in the spectral region of our experiment.

5. Summary

We propose and demonstrate resonant plasmonic nano-comb structures for efficient large-area nonlinear effects. For the 1.0 μm spacing PNCs under the fixed-pump-power condition, the nonlinear SHG power shows the pump-size-independency over a range of pump diameters of 2~6 μm. Over 200-fold increase of nonlinear signal is observed for the pump beam diameter of 6 μm. We claim that the resonant coupling of the finite-size pump wave with the finite-size one-dimensional plasmonic mode is responsible for this interesting phenomenon. The proposed plasmonic nano-comb structure could be applicable to energy efficient, large-area nonlinear optical devices and biological sensors.

Acknowledgments

The authors would like to thank Dr. Kipom Kim for his providing the analysis tool for the electron-multiplication charge-coupled device. This work was supported by the National Research Foundation of Korea (NRF) Grants (2013K1A1A2035662, 2007-0093863). M.-K Kim acknowledges the support of the Basic Science Research Program through the National Research Foundation of Korea (NRF) (2014R1A1A1008604).